Thermochimica Acta 507–508 (2010) 49–59

Contents lists available at ScienceDirect

Thermochimica Acta

journal homepage: www.elsevier.com/locate/tca

Investigation of thermal degradation of some ferrocene liquid crystals

Gabriela Lisa[a,*], Daniela Apreutesei Wilson[a,b], Dan Scutaru[a], Nita Tudorachi[c], Natalia Hurduc[d]

[a] "Gh. Asachi" Tehnical University, Iaşi, Faculty of Chemical Engineering and Environmental Protection, 71 D, Mangeron Blv, 700050 Iaşi, Romania
[b] Roy & Diana Vagelos Laboratories, Department of Chemistry, University of Pennsylvania, Philadelphia, Pennsylvania 19104-6323, USA
[c] Petru Poni" Institute of Macromolecular Chemistry, Aleea Gr. Ghica Voda 41A, 700487 Iasi, Romania
[d] "Al. I. Cuza" University, Iaşi, Faculty of Chemistry, 11 Carol I Blv, 700506 Iasi, Romania

ARTICLE INFO

Article history:
Received 11 January 2010
Received in revised form 29 April 2010
Accepted 30 April 2010
Available online 11 May 2010

Keywords:
Ferrocene liquid crystals
Thermal degradation
TG–MS–FTIR

ABSTRACT

The present study regarding the thermal behavior of some ferrocene derivatives with liquid crystal properties is aimed at evaluating the relationship between structure–thermostability–degradation mechanism, leading to information about their applications, processing parameters and industrial waste recycling procedures. The thermostability series of some ferrocene derivatives bearing the ferrocenyl unit rigidly connected to the mesogen and of some analogous phenyl compounds were established; the influence of the connecting groups, the ferrocene and the cholesterol units upon the thermal stability was investigated.

1. Introduction

The physical and chemical properties of materials are mainly determined by the functional unit combinations contained within their structure. In organometallic molecules the most important factor is the presence of the metal that contributes not only with its own properties, but also brings molecular arrangements that are not found in other organic derivatives [1–4]. The thermal stability of a newly synthesized compound is an important feature affecting its practical applications, especially in those fields in which high temperature processing is required. One of the most desired properties of the newly synthesized materials is their thermal stability. Due to the fact that in thermotropic materials the liquid crystal ordering occurs in a certain temperature range, it is obvious that their thermal stability plays a crucial role. While the thermal stability of the polymeric liquid crystals has been intensely studied [5–12], small molecule liquid crystals on the other hand have been comparatively less studied with respect to their thermostability [13–19]. Due to their simpler molecular structure, they allow better understanding of the degradation processes and their systematic study may contribute important information [20–22].

With all the above considerations in mind, we set the main objective of this work on elucidating the molecular structure influence upon the thermal stability of a series of ferrocene derivatives with the ferrocene moiety rigidly connected to the mesogen unit and also of some analogous phenyl derivatives. The thermal stability study of these compounds is motivated by the presence of high transition temperatures and even more by the fact that their isotropic transition temperatures are situated above their thermal stability range.

2. Experimental

2.1. Materials

Ferrocene derivatives containing cholesterol rigidly connected to the mesogen unit were obtained either by esterification of the ferrocene unit with the mesogen using DCC/DMAP, or by condensation of ferrocene amines with cholesterol containing aldehydes [23,24].

2.2. Equipment

Thermogravimetric measurements (TGA) were performed on a Mettler Toledo TGA-SDTA851e derivatograph (thermogravimetric analyzer) under a flow of nitrogen and air (20 ml/min), in the temperature range 25–900 °C, and a heating rate of 10 K min^{-1} with 4–6 mg of sample mass. The operational parameters were kept constant for all samples in order to obtain comparable data.

Thermal degradation of some ferrocene liquid crystals and evolved gas analyses were performed using a TG/FTIR/MS system. The system is equipped with an apparatus of simultaneous thermogravimetric spectrophotometer FTIR model Vertex-70 (Bruker-Germany) and mass spectrometer model QMS 403C Aëolos (Netzsch-Germany). Samples with weight ranging from 3 to 8 mg were heated from 25 to 600 °C, at a heating rate of 10 °C/min.

* Corresponding author. Tel.: +40 232 278683; fax: +40 232 271311.
E-mail addresses: gapreot@yahoo.com, gapreot@ch.tuiasi.ro (G. Lisa).

0040-6031/$ – see front matter © 2010 Elsevier B.V. All rights reserved.
doi:10.1016/j.tca.2010.04.030

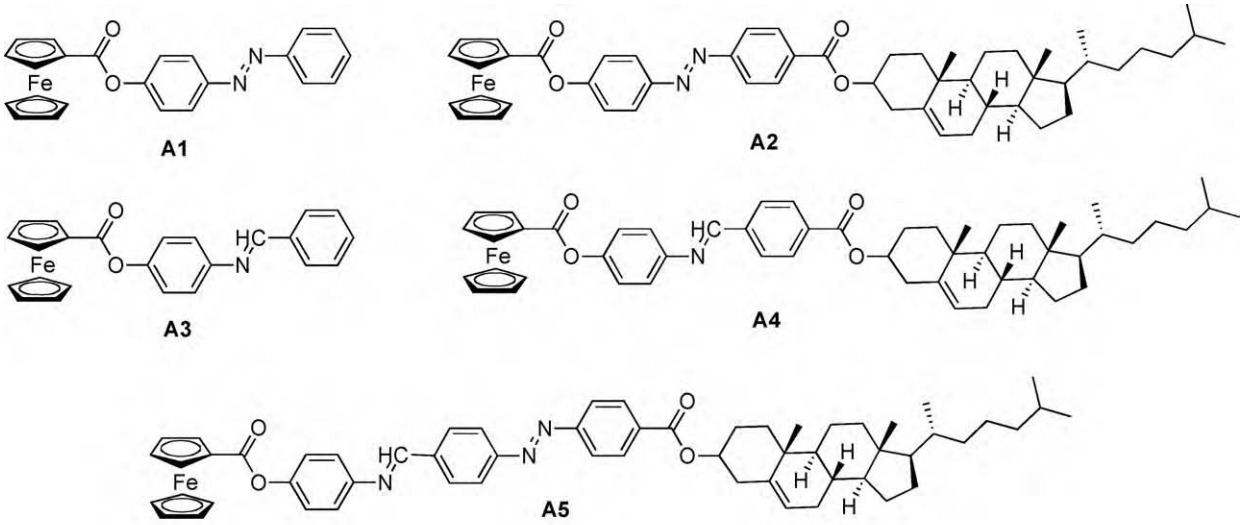

Class A compounds

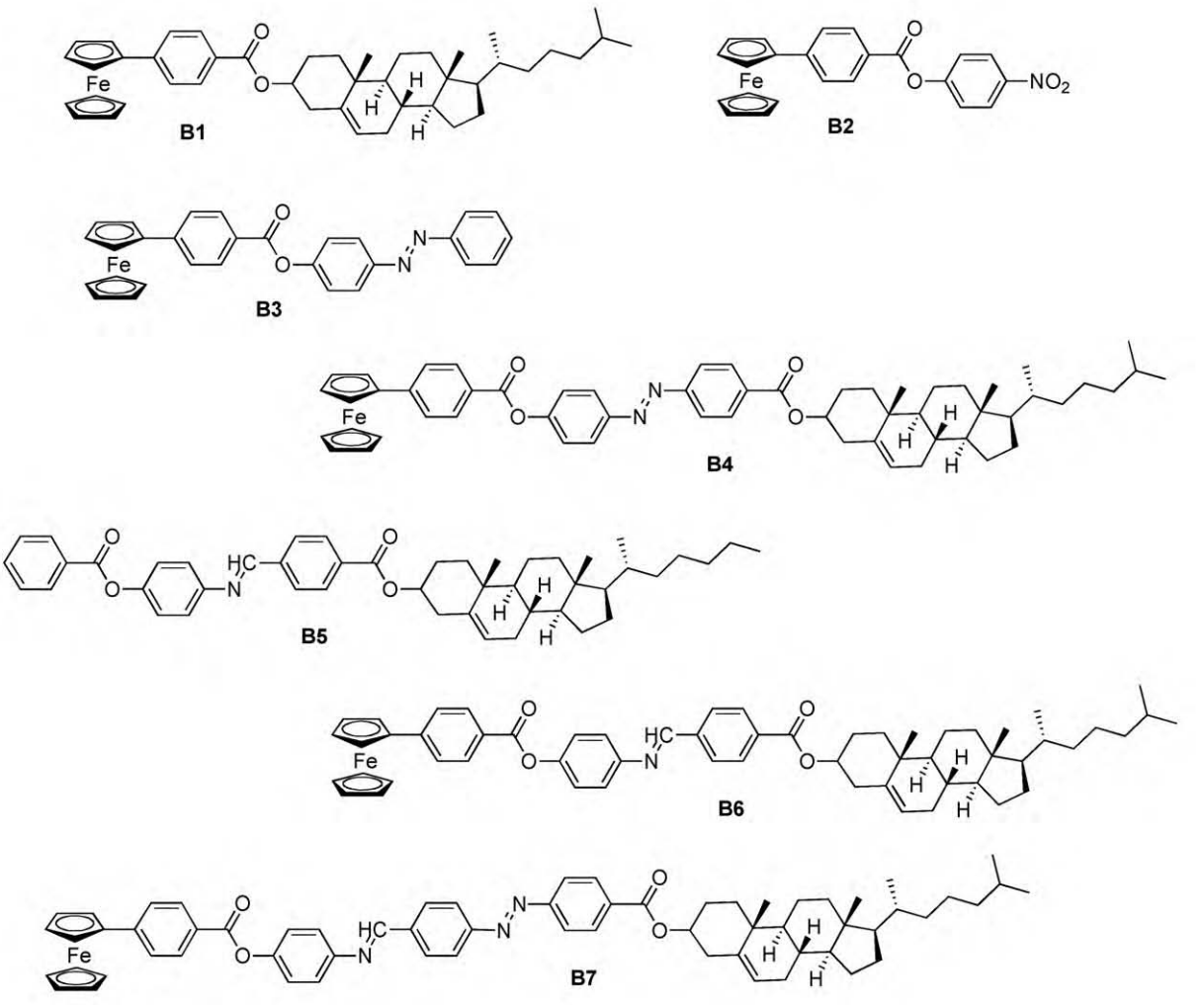

Class B compounds

Scheme 1. The chemical structure of the ferrocene derivatives.

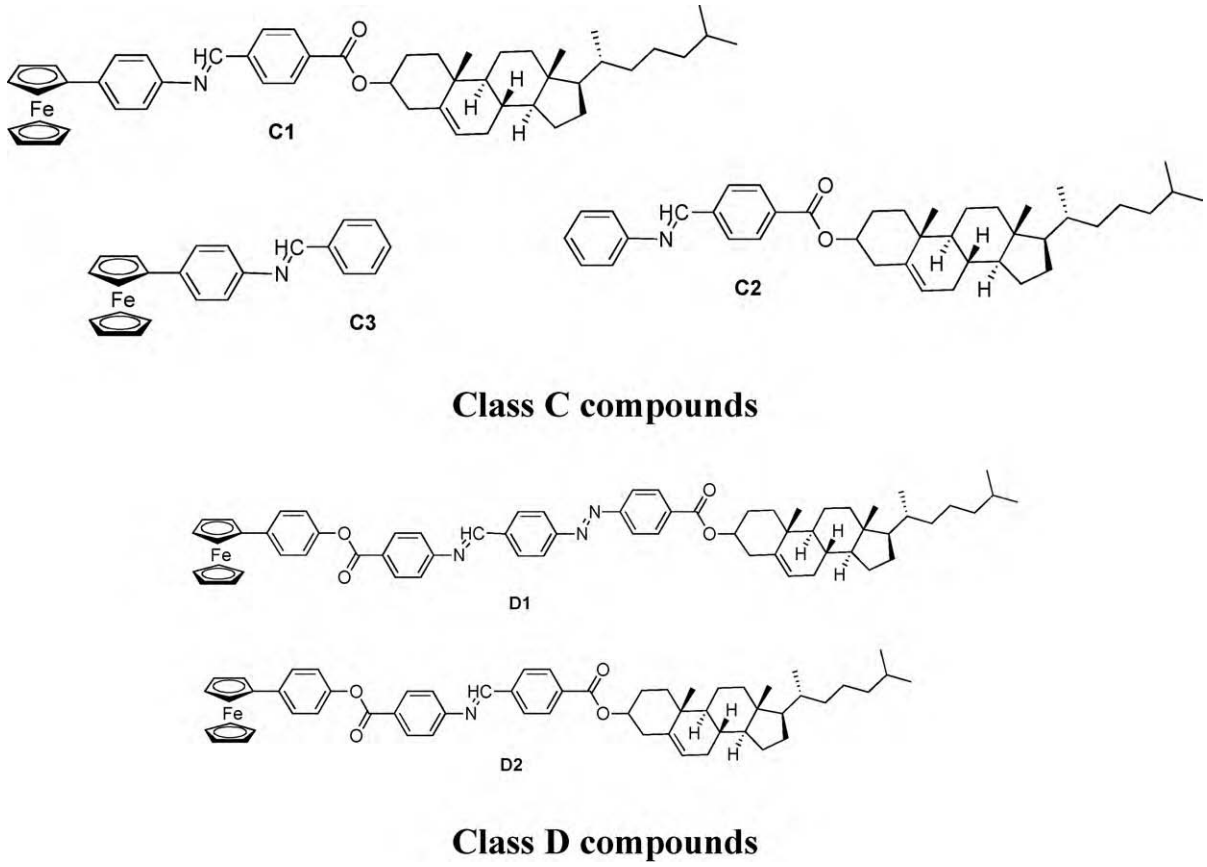

Scheme 1. (*Continued*).

The helium as carrier gas with flow rate of 50 ml/min and protective purge for thermobalance of 20 ml/min was used. The gases released during thermal decomposition processes are transferred by two isothermal transition lines to FTIR and mass spectrometer. The gases are introduced in TGA-IR external modulus of FTIR spectrophotometer, and FTIR spectra are recorded from 600 to 4000 cm^{-1} with a resolution of 4 cm^{-1}. The transfer gases line to mass spectrometer is manufactured from quartz. The mass spectra were recorded under the electron impact ionization energy of the 70 eV. The acquisition of data was recorded with Aeolos® 7.0

Table 1
Thermogravimetric characteristics for **A** type compounds.

Sample	Stage	Nitrogen atmosphere				Air			
		T_{onset} (°C)	T_{peak} (°C)	T_{endset} (°C)	W%	T_{onset} (°C)	T_{peak} (°C)	T_{endset} (°C)	W%
A1	I	287	300	315	33.64	305	320	348	29.04
	II	382	410	454	18.96	348	440	580	53.60
	III	601	624	654	14.31	–	–	–	–
	Residue				33.09				17.36
A2	I	306	317	365	18.97	335	377	405	32.68
	II	365	374	383	27.14	405	534	630	36.91
	III	420	443	466	21.60	715	770	895	18.47
	IV	647	654	704	16.51	–	–	–	–
	Residue				15.78				11.94
A3	I	296	309	316	11.87	302	317	350	19.26
	II	361	406	416	16.80	350	488	728	69.41
	III	434	444	480	10.63	–	–	–	–
	IV	636	658	706	24.28	–	–	–	–
	Residue				36.42				11.33
A4	I	315	344	374	47.07	272	379	405	33.35
	II	432	464	484	23.14	405	434	481	30.44
	III	650	660	673	14.36	481	552	671	24.35
	Residue				15.43				11.86
A5	I	277	310	332	33.66	271	312	375	16.59
	II	368	396	404	15.11	455	500	580	41.42
	III	421	433	470	18.24	580	600	770	29.76
	IV	630	652	760	18.24	–	–	–	–
	Residue				14.75				12.23

Table 2
Thermogravimetric characteristics for B type compounds.

Sample	Stage	Nitrogen atmosphere				Air			
		T_{onset} (°C)	T_{peak} (°C)	T_{endset} (°C)	W%	T_{onset} (°C)	T_{peak} (°C)	T_{endset} (°C)	W%
B1	I	309	342	357	51.24	308	400	415	13.21
	II	418	455	479	14.49	445	485	517	41.40
	III	610	640	734	15.17	517	544	708	29.52
	Residue				19.10				15.87
B2	I	123	170	208	5.13	120	263	303	15.58
	II	208	228	247	7.59	380	518	580	25.10
	III	390	418	431	9.06	580	662	895	50.85
	IV	460	475	534	7.22	–	–	–	–
	V	679	738	758	16.81	–	–	–	–
	Residue				54.19				8.47
B3	I	287	299	306	15.39	308	392	380	8.82
	II	373	437	449	6.11	440	558	590	30.72
	III	486	491	495	5.89	590	796	880	37.94
	IV	624	726	744	19.45	–	–	–	–
	Residue				53.16				22.52
B4	I	316	325	343	13.38	334	374	430	13.72
	II	389	415	421	26.58	430	471	580	42.23
	III	421	456	486	21.99	580	670	760	29.03
	IV	619	627	751	17.13	–	–	–	–
	Residue				20.92				15.02
B5	I	320	345	370	67.30	300	398	440	41.40
	II	425	441	491	21.96	440	496	560	37.81
	III	–	–	–	–	560	784	900	20.31
	Residue				10.74				0.48
B6	I	317	361	383	39.25	315	356	420	10.08
	II	432	467	484	24.81	420	443	580	45.69
	III	622	641	665	5.57	580	600	780	34.51
	IV	761	776	800	2.95	–	–	–	–
	Residue				27.42				9.72
B7	I	274	287	327	22.37	300	325	370	11.31
	II	376	410	437	18.86	380	497	570	33.60
	III	451	462	483	14.18	570	610	773	42.58
	IV	629	711	770	22.56	–	–	–	–
	Residue				22.03				12.51

software, in spectrum scanning (SCAN) mode scan bar graph in the range of m/z = 1–300, measuring time was ca. 0.5 s for one channel, resulting in time/cycle of approximately 150 s.

3. Results and discussion

The chemical structures of the ferrocene derivatives for which the thermal stability was analyzed are presented in Scheme 1. These compounds contain both mesogen units connected by azo or imino-aromatic groups and cholesteryl units. Each structural unit brings its own contribution to the overall material properties: *ferrocene* – allows formation of unique geometries, not found in other organic compounds [25]; *cholesterol* – by its optical activity provides helical molecular arrangements; *azo groups* – allow photochemical changes in the cholesteric step by *trans–cis* isomerisation. Due to the important advantages induced by the presence of the chirality, the ferrocene and the azo unit, it is obvious that these structures may become suitable precursors for obtaining new materials that respond to magnetic and electric field changes or to UV/vis radiation.

Nearly all of the proposed compounds show mesomorphic properties as a consequence of the pro-mesogenic character of the cholesteryl unit [26,27]. Since this group determines compact molecular packing in solid state by strong intermolecular interactions, the melting point increases significantly, sometimes beyond the thermal stability range [28]. Due to the fact that most

Table 3
Thermogravimetric characteristics for **C** type compounds.

Sample	Stage	Nitrogen atmosphere				Air			
		T_{onset} (°C)	T_{peak} (°C)	T_{endset} (°C)	W%	T_{onset} (°C)	T_{peak} (°C)	T_{endset} (°C)	W%
C1	I	319	375	394	45.50	340	371	401	14.61
	II	410	462	486	19.65	440	480	566	39.78
	III	649	655	708	8.56	566	656	765	35.81
	IV	844	853	900	8.85	–	–	–	–
	Residue				17.44				9.80
C2	I	320	358	374	63.00	365	446	480	52.06
	II	374	450	516	10.77	480	630	700	23.47
	Residue				26.23				24.47
C3	I	309	417	433	91.71	400	473	520	51.57
	II	647	652	730	5.79	520	604	760	32.13
	Residue				2.50				16.30

Table 4
Thermogravimetric characteristics for **D** type compounds.

Sample	Stage	Nitrogen atmosphere				Air			
		T_{onset} (°C)	T_{peak} (°C)	T_{endset} (°C)	W%	T_{onset} (°C)	T_{peak} (°C)	T_{endset} (°C)	W%
D1	I	273	298	361	39.58	340	363	380	11.87
	II	397	434	479	24.03	405	503	595	44.40
	III	661	689	748	15.25	600	717	775	39.53
	Residue				21.14				4.20
D2	I	325	342	365	24.29	350	370	403	21.16
	II	365	381	393	20.38	403	440	480	37.19
	III	426	460	479	13.70	480	595	760	25.89
	IV	634	649	760	22.01	-	-	-	-
	Residue				19.62				15.76

of the analyzed compounds show isotropisation points located over their thermal stability limit, high exothermic peaks are evidenced in the DSC curves, corresponding to high degradation temperatures for the samples. As a result of the thermal decomposition process, the characteristic peaks for the transition from liquid to liquid crystal state, are almost impossible to detect upon cooling. This is due to the low enthalpy of the transition to liquid crystal state, but also to the fact that the initiation of the degradation process, that is exothermic, masks the endothermic effect.

As a result of systematically modifying the chemical structure, it is possible to elucidate the influence of various structural factors by performing thermal stability comparative analysis on the investigated compounds. The effects of the bonding groups, the ferrocene and the cholesterol units were explored.

The influence of the bonding groups was investigated by comparing the thermal stability of the ferrocene derivatives having similar length of the mesogenic block, but different ester or imine groups that connect it to the ferrocenyl or cholesteryl unit. For elucidating the influence of the ferrocene unit the thermal stability of compounds with similar length mesogenic groups but containing no ferrocene were compared (**B6** with **B5** or **C1** with **C2**). The analysis of the cholesterol presence may be performed by comparing the thermostability of the following pairs: **A1** with **A2**; **A3** with **A4**; or **B3** with **B4**.

The thermogravimetric curves indicate a complex degradation mechanism which takes place in 2–5 stages, depending on the chemical structure of the analyzed compounds and on the atmosphere in which the process proceeds. For all samples complete degradation was not observed; the amount of residue being up to 54% of the sample both in air and in nitrogen. The lowest residue amount, below 5% of the sample weight, was recorded for sample **B5** in air and **C3** in nitrogen.

The thermogravimetric characteristics: T_{onset} – the temperature at which the thermal degradation begins, T_{peak} – the temperature at which the thermal degradation is maximum, T_{endset} – the temperature at which the process is complete and W% – the weight percentage loss recorded in each stage are presented in Tables 1–4 and refers to the four classes of derivatives that contain ferrocene rigidly connected to the mesogenic unit.

For comparing the thermostability of the analyzed compounds, the temperature at which the thermal degradation begins (T_{onset}) was considered.

Taking into account the T_{onset} temperature, the following thermal stability series were established:

- In inert atmosphere (N_2)
  - **A5 < A1 < A3 < A2 < A4**
  - **B2 < B7 < B3 < B1 < B4 ≅ B6 < B5**
  - **C3 < C1 ≅ C2**
  - **D1 < D2**
- In air
  - **A5 ≅ A4 < A3 < A1 < A2**
  - **B2 < B7 = B5 < B3 = B1 ≪ B6 < B4**
  - **C1 < C2 < C3**
  - **D1 < D2**

These results show inversions in the thermostability series depending on the atmosphere in which the thermal degradation of the ferrocene derivatives took place, in compounds belonging to classes A, B and C.

The thermostability change as a function of the thermal degradation atmosphere depends on the mode of connecting the ester group to the ferrocene and on the number of linking groups. While in the class A and B compounds the differences are small, they become significant in the class C compounds.

Given the importance of the cholesterol in inducing the liquid crystal properties, but also due to the strong interactions between cholesteryl residues that leads to compact packing patterns and high melting points, a further study of selected compounds by TG–MS–FTIR analysis was performed on compounds: **A4**, **B4** and **A3**, **B3**. These compounds have comparable structures, the only difference being the presence or absence of the cholesteryl unit. The thermogravimetric curves were recorded in helium and the thermal characteristics are presented in Table 5. The DTG curves are shown in Figs. 1–4, by comparison with the ones obtained in air and nitrogen, respectively, in order to evidence the influence of the atmosphere in which the decomposition took place. Although the same decomposition stage sequence was obtained in helium as in nitrogen, the processes are better delimited in helium. For example, in sample **A3**, in the temperature range of 430–480 °C the decomposition in helium tends to show two separate processes, compared to a single one in nitrogen. The differences are more significant when

Table 5
Thermogravimetric characteristics for the compounds analyzed in helium: **A3**, **A4**, **B3** and **B4**.

Sample	Stage	T_{onset} (°C)	T_{peak} (°C)	T_{endset} (°C)	W%
A3	I	283	305	319	27.45
	II	371	397	426	7.86
	III	438	443	489	14.94
	Residue				49.75
A4	I	306	328	394	55.43
	II	436	459	486	16.71
	Residue				27.86
B3	I	285	301	322	24.63
	II	322	361	404	4.20
	III	404	451	486	7.71
	Residue				63.46
B4	I	295	317	334	41.38
	II	390	397	433	4.71
	III	433	440	498	12.82
	Residue				41.09

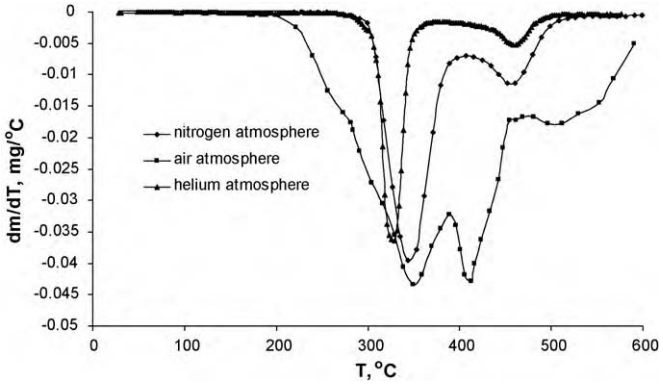

Fig. 1. DTG curves obtained for sample **A4**.

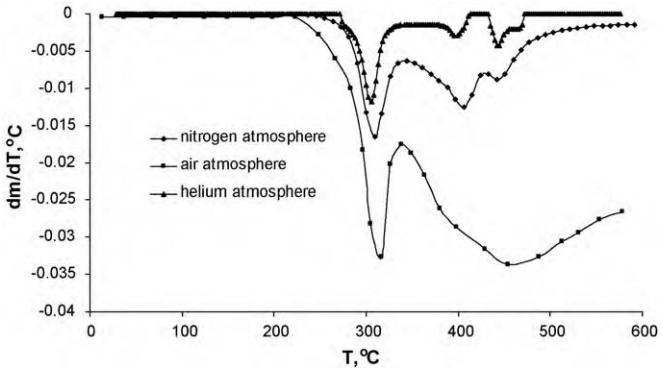

Fig. 2. DTG curves obtained for sample **A3**.

the decomposition is performed in air. The residue left at 600 °C is a few percentage points less in air compared to inert gases, which is proof that the thermo oxidation is favored by the presence of oxygen in air.

The recorded MS curves allowed ionic fragment identification in the temperature range of 30–600 °C. Partial results obtained for sample **A3** are presented in Fig. 5.

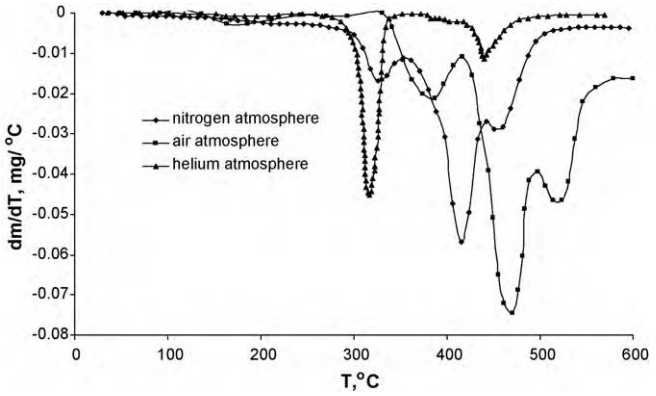

Fig. 3. DTG curves obtained for sample **B4**.

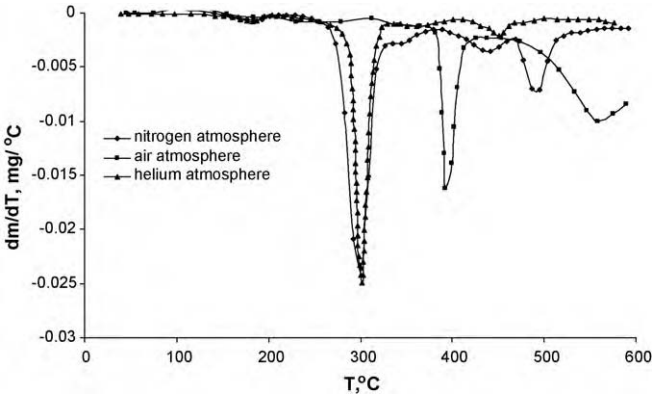

Fig. 4. DTG curves obtained for sample **B3**.

The MS results show that the thermal degradation seems to be initiated on the cyclopentadienyl groups belonging to ferrocene. In the first degradation stage (Fig. 5) of sample **A3** in the temperature range of 280–320 °C, a maximum ion beam is obtained for the fragments with the mass to charge ratios $m/z = 65$ and $m/z = 66$. The

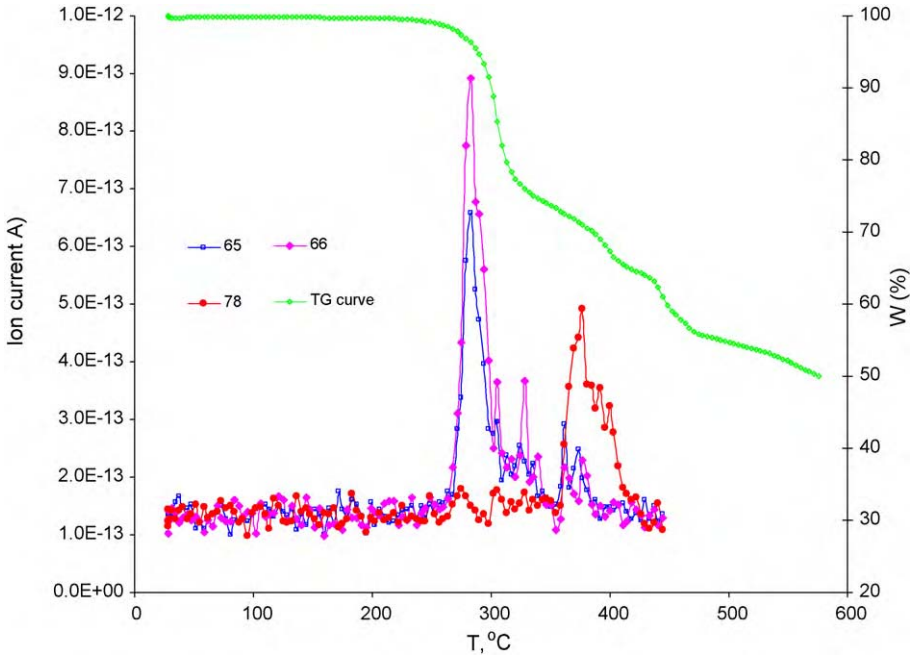

Fig. 5. TG and MS comparative results for sample **A3**.

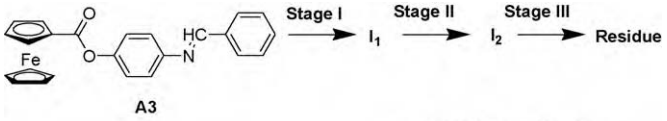

Stage I

Mass/Charge m/z	Species
65	$C_5H_5^+$
66	$C_5H_6^+$

Stage II and Stage III

Mass/Charge m/z	Species
44	CO_2^+
28	$HCNH^+$
78	$C_6H_6^+$

Scheme 2. Identified fragments during the thermal degradation of A3 (TG–MS investigations).

identified fragments, appearing during the thermal degradation of sample A3 (TG–MS investigations) are shown in Scheme 2. Fig. 6 presents FTIR spectra at different temperatures based on the corresponding maxima on Gram Schmidt graph (Fig. 7). The bands at 2361 cm^{-1} and 2342 cm^{-1}, respectively are characteristic for CO_2 [28], while the band located at 662 cm^{-1} can be assigned to the vibration of the cyclopentadienyl ion [29]. While the temperature increases and the degradation proceeds to stages II and III, the signal characteristic to CO_2 intensifies (fragment 44 on the MS spectrum) while the 662 cm^{-1} peak characteristic to the cyclopentadienyl ion disappears.

Partial MS results for sample **A4** are presented in Fig. 8. The thermal degradation is initiated on the cyclopentadienyl groups belonging to the ferrocene as well, but the process occurs at higher temperature. The degradation continues with the split of the connecting groups and the aromatic rings evidenced by the presence of the ionic fragments with ratios $m/z = 39$ and $m/z = 40$. In the second step the terminal groups belonging to cholesteryl are also split resulting in MS peaks with ratios of $m/z = 41$, 42 and 43, respectively. The identified fragments, appearing during the thermal degradation of sample A4 (TG–MS investigations) are presented in Scheme 3. In the FTIR spectra corresponding to the temperatures at which maxima of the Gram Schmidt graph are detected (Fig. 7), bands characteristic to vibration of bonds CO_2, –CH, =CH,

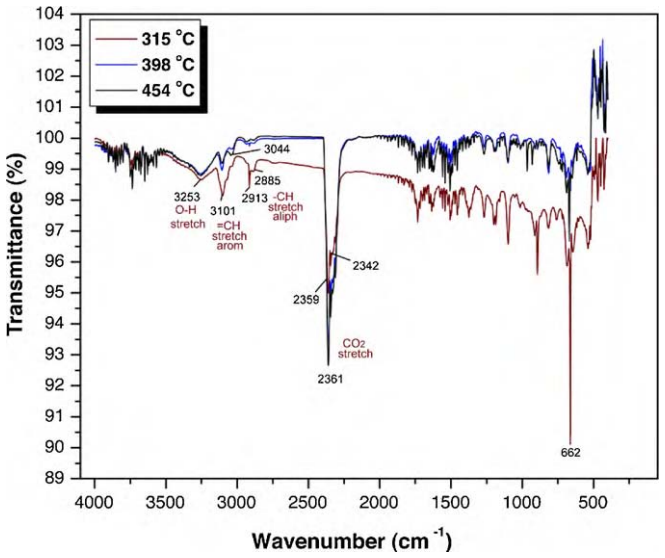

Fig. 6. FTIR spectrum of sample **A3**.

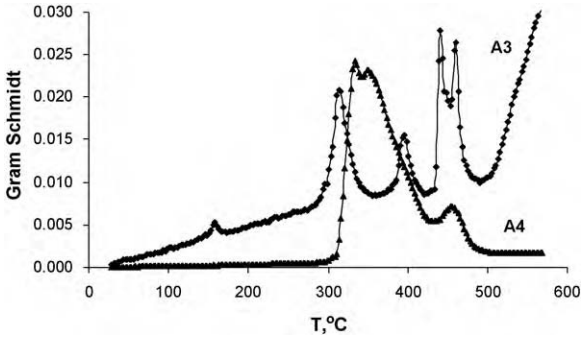

Fig. 7. Gram Schmidt graph of samples **A3** and **A4**.

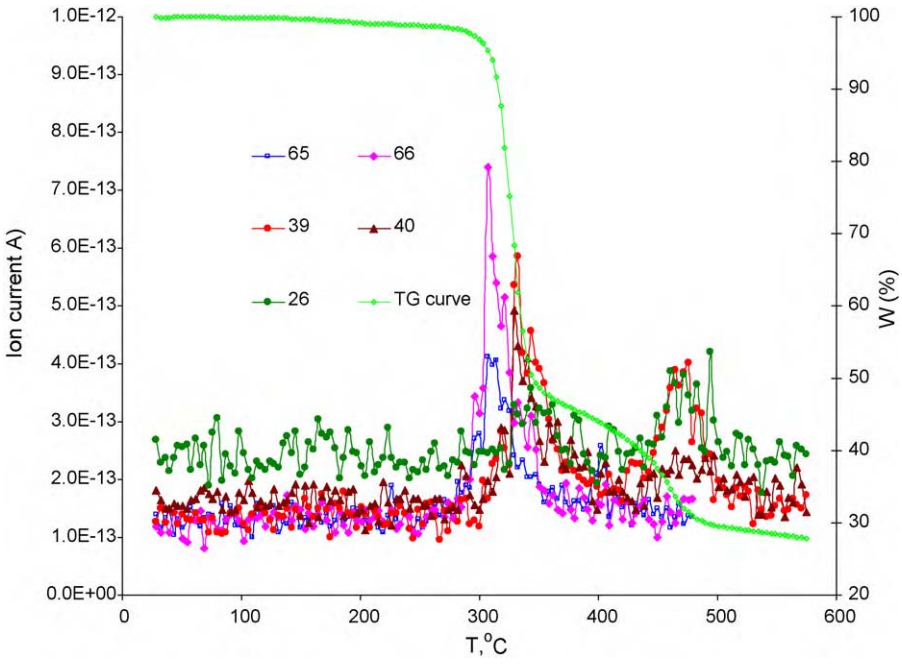

Fig. 8. TG and MS comparative results for sample **A4**.

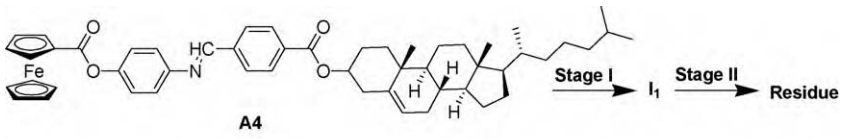

A4

Stage I

Mass/Charge m/z	Species
65	$C_5H_5^+$
66	$C_5H_6^+$
44	CO_2^+
39	$C_3H_3^+$
40	$C_3H_4^+$
26	CN^+

Stage II

Mass/Charge m/z	Species
78	$C_6H_6^+$
44	CO_2^+
15	$CH3^+$
41	$C_3H_5^+$
42	$C_3H_6^+$
43	$C_3H_7^+$
70	$C_5H_{10}^+$

Scheme 3. Identified fragments during the thermal degradation of **A4** (TG–MS investigations).

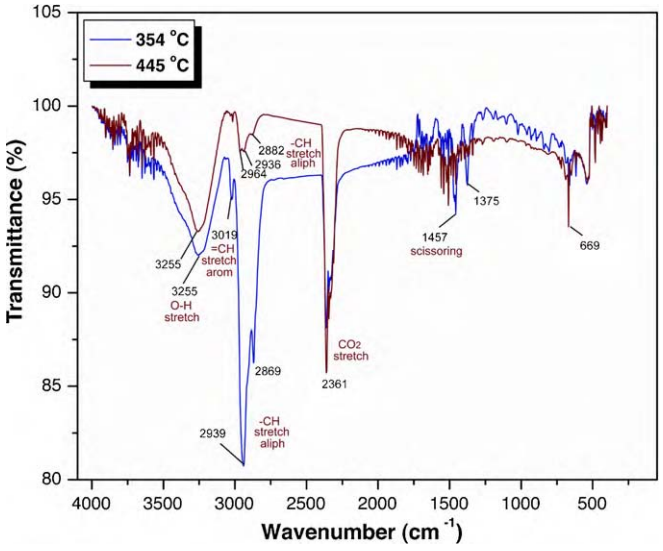

Fig. 9. FTIR spectrum of sample **A4**.

are detected, also in addition to the vibration of the cyclopentadienyl ion (Fig. 9).

The analysis of the MS curves for compound **B3** obtained by esterification of acids with ferrocene containing azo-phenol and that does not contain cholesterol, indicated that the initiation of the thermal degradation takes place at the –N=N– group and continues with aromatic and other connecting group splitting. TG curve and MS spectra obtained for fragments with ratios $m/z = 28$ and respectively $m/z = 44$ are presented as an example in Fig. 10.

The identified fragments, appearing during the thermal degradation of sample **B3** (TG–MS investigations) is indicated in Scheme 4. The FTIR spectra for the temperatures that correspond to maxima on the Gram Schmidt graph (Fig. 11), in the 300–440 °C range, are presented in Fig. 12, confirming that the thermal degradation process occurs according to Scheme 4.

The thermal degradation of sample B4 in helium begins at 295 °C with CO_2 emission, followed by aromatic residue splitting. The degradation process continues with N_2 emission and then, in the following stages, the terminal groups belonging to cholesteryl are split, resulting in MS peaks at ratios $m/z = 41, 42$ and 43, respectively (Fig. 13). The identified fragments, appearing during the thermal degradation of sample **B4** (TG–MS investigations) are presented in Scheme 5.

FTIR spectra for sample **B4** at the two temperature values that show maxima on the Gram Schmidt graph (Fig. 11) are presented in Fig. 14. Characteristic bands for vibration mode of the bonds CO_2, O–H, –CH, are observed.

Structural modifications of the analyzed compounds allowed complete evaluation of the influence of various factors such as: the connecting groups, the ferrocene and the cholesterol units upon the thermal stability.

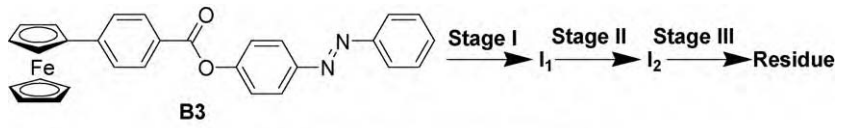

B3

Mass/Charge m/z	Species
28	N_2^+
44	CO_2^+
39	$C_3H_3^+$
40	$C_3H_4^+$

Scheme 4. Identified fragments during the thermal degradation of **B3** (TG–MS investigations).

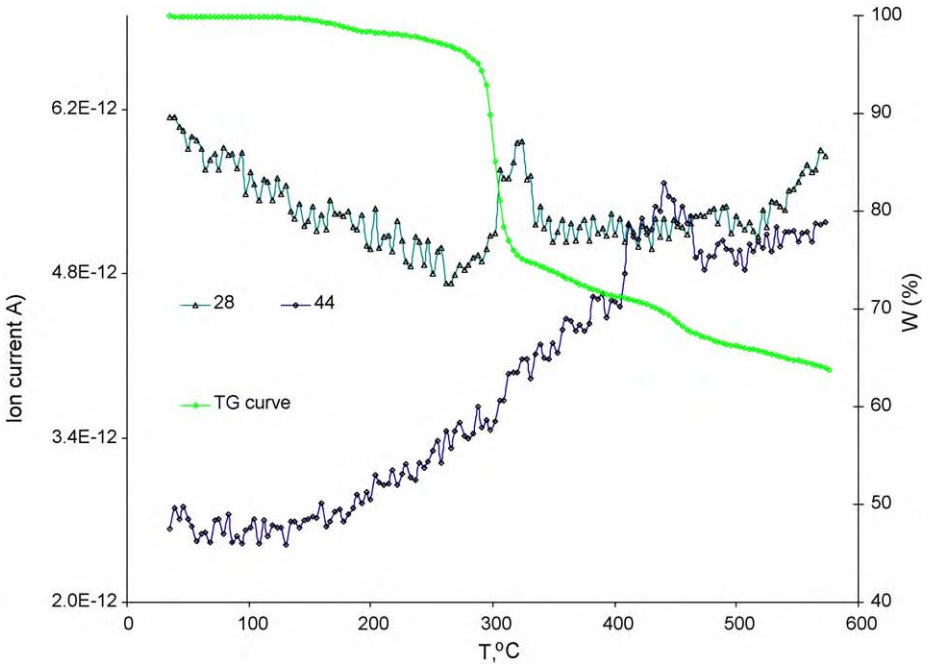

Fig. 10. TG and MS comparative results (ion current 10^{-12}) for sample **B3**.

3.1. The influence of the connecting groups

The ferrocene derivatives that contain an ester group with electron attracting effect immediately adjacent to the ferrocenyl unit **A2**, **A3** and **A4** display a lower thermostability than the azo-derivative **B4** or the Schiff bases, **C3**, **B6** and **C1**, in which the ferrocene has an aromatic ring attached to it. A possible explanation might be the fact that such a group in conjugation with the cyclopentadienyl ring belonging to the ferrocene, induces a destabilization of the retroactive π bond located between the iron atom and the two ferrocene rings, thus resulting in a decrease of the thermostability. The destabilization effect of the ferrocenyl group is confirmed by the mass spectrometry analysis performed on the compounds containing a carboxyl function adjacent to the ferrocenyl (i.e. **A3** and **A4**) by comparison with the compounds that contain a phenyl group adjacent to the ferrocenyl (i.e. **B3** and **B4**). The fragments with masses 65 and 66, respectively characteristic to the pentadienyl group were detected in the first degradation stage of samples **A3** and **A4**, but were missing in samples **B3** and **B4**.

3.2. The influence of the ferrocene

By comparing the characteristic temperatures for the compounds containing ferrocene **B6**, **C1** with the homologous derivatives that do not contain this group **B5**, **C2** the fact that they have comparable thermostabilities becomes notice-

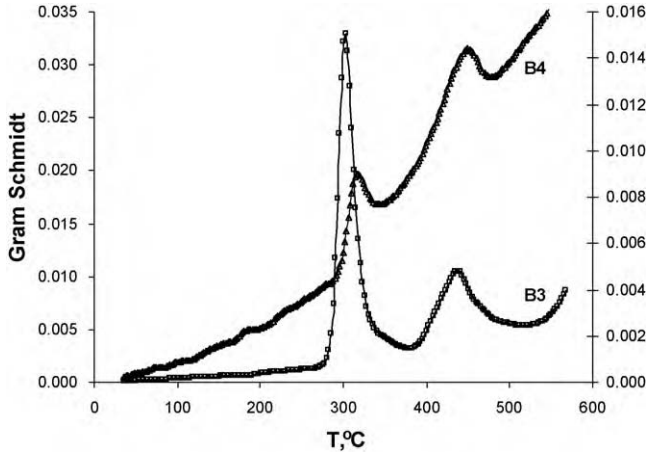

Fig. 11. Gram Schmidt graph for samples **B3** and **B4**.

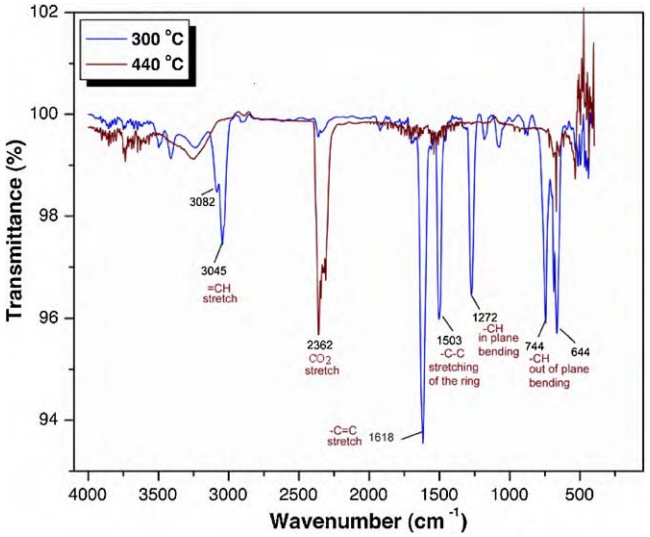

Fig. 12. FTIR spectrum for sample **B3**.

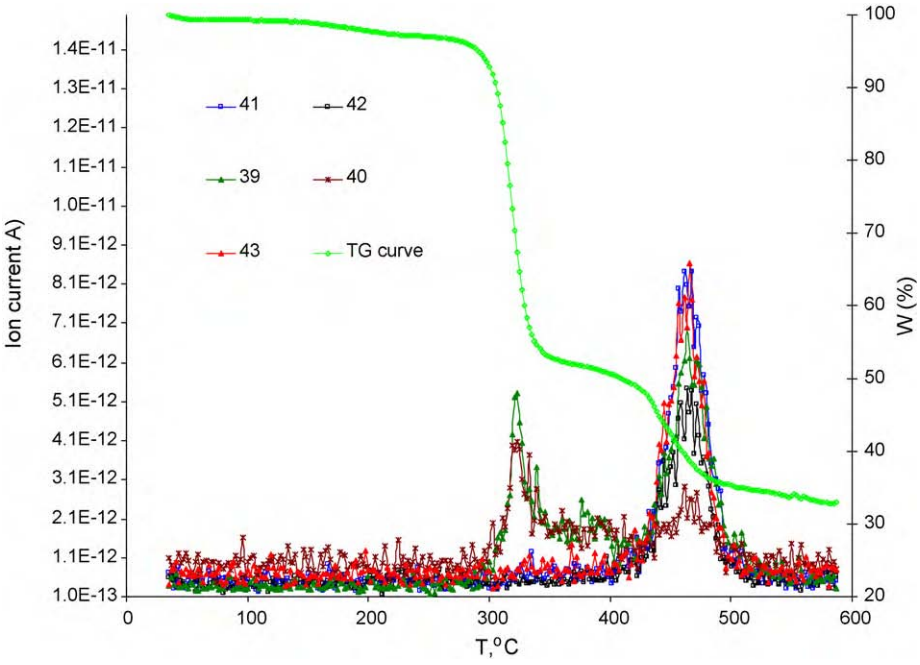

Fig. 13. TG and MS comparative results for sample **B4**.

able. This is probably due to the fact that the thermal degradation is initiated by the –N=CH– groups which are present in both structures, whether they contain ferrocene or not.

3.3. The influence of the cholesterol

The presence of the cholesterol leads in most cases to a slight increase in thermostability. By comparing the characteristic temperatures of the compounds without cholesterol **A2**, **A4**, **B4**, **C1** with the homologous derivatives that contain this unit **A2**, **A4**, **B4**, **C1**, the fact that the thermostability is about 10 °C higher in the latter becomes obvious. When estimating the thermal stability, it is important to consider not a single molecule, but its neighbors as well because the intermolecular forces also contribute to the thermal stability. These interactions can affect the melting points and therefore state of matter of a certain material at a given temperature [27].

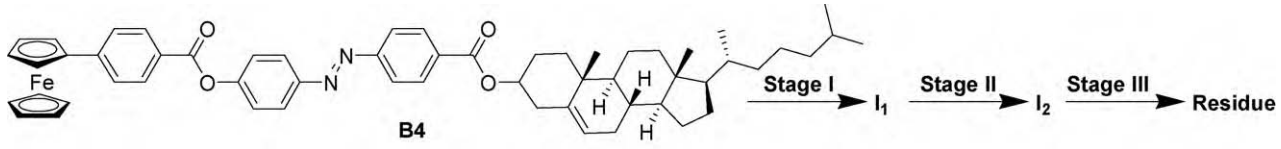

Mass/Charge m/z	Species
28	N_2^+
44	CO_2^+
39	$C_3H_3^+$
40	$C_3H_4^+$
15	CH_3^+
41	$C_3H_5^+$
42	$C_3H_6^+$
43	$C_3H_7^+$

Scheme 5. Identified fragments during the thermal degradation of **B4** (TG–MS investigations).

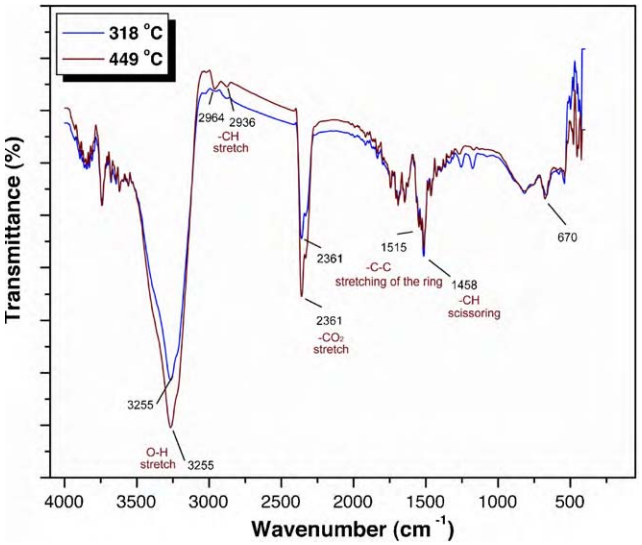

Fig. 14. FTIR spectrum of sample **B4**.

4. Conclusions

The observations regarding the correlation structure–thermostability–degradation mechanism and the influence of the atmosphere in which the thermal degradation takes place indicate the possibility of directing the synthesis towards certain routes for obtaining compounds with liquid crystal properties. The thermostability series were determined for the four classes of analyzed compounds. The influence of the connecting groups, the ferrocene and the cholesterol units upon the thermal stability was also elucidated. The results of the TG–MS–FTIR analyses show that when the compounds contain an ester group with electron attracting effect immediately adjacent to the ferrocenyl unit, their thermostability is reduced compared to the compounds in which the phenyl group is attached to the ferrocenyl unit. This finding may be explained by the fact that such a group that is in conjugation with the cyclopentadienyl ring belonging to the ferrocene induces a destabilization of the retroactive π bond established between the iron atom and the two pentadienyl groups of the ferrocene, thus initiating thermal degradation on these pentadienyl groups. In compounds containing the phenyl group directly attached to the ferrocenyl the initiation of the thermal degradation takes place at the connecting groups between the aromatic rings. The presence of the cholesterol leads in most cases to a slight increase in thermostability due to compact molecular packing in solid state caused by strong interactions between the cholesteryl units.

Acknowledgements

This work was supported by CNCSIS – UEFISCSU, project number PNII – IDEI 600/2007.

References

[1] O.N. Kadkin, E. Ho Kim, So.Y. Kim, M.-G. Choi, Polyhedron 28 (2009) 1301.
[2] T. Seshadri, H. Ju, R. Haupt, U.F. Rke, G. Henkel, Liq. Cryst. 34 (1) (2007) 33.
[3] C. Hye Won, K. Oleg, C. Moon-Gun, Liq. Cryst. 36 (1) (2009) 53.
[4] O.N. Kadkin, H. Han, Y.G. Galyametdinov, J. Organomet. Chem. 692 (2007) 5571.
[5] N. Hurduc, A. Creangă, D. Scutaru, S. Alazaroaie, Natalia Hurduc, Rev. Roum. Chim. 47 (2002) 1.
[6] A. Creangă, G. Pokol, N. Hurduc, Cs. Novak, S. Alazaroaie, Natalia Hurduc, J. Therm. Anal. Calorim. 66 (3) (2001) 859.
[7] N. Hurduc, A. Creanga, G. Pokol, Cs. Novak, D. Scutaru, S. Alazaroaie, Natalia Hurduc, J. Therm. Anal. Calorim. 70 (2002) 877.
[8] C. Damian, N. Hurduc, N. Hurduc, R. Shanks, D. Pavel, Comp. Mater. Sci. 27 (2003) 393.
[9] D.R. Mulligan, C.T. Imrie, P. Larcey, J. Mater. Sci. 31 (1996) 1985.
[10] D. Jayalatha, R. Balamurugan, P. Kannan, High Perform. Polym. 21 (2009) 139.
[11] D. Filip, C.I. Simionescu, D. Macocinschi, J. Serb. Chem. Soc. 66 (2001) 153.
[12] Z. Akhter, M.A. Bashir, M. Saif ullah Khan, Appl. Organomet. Chem. 19 (2005) 848.
[13] D. Apreutesei, G. Lisa, N. Hurduc, D. Scutaru, CEJC 2 (2004) 553.
[14] D. Apreutesei, G. Lisa, N. Hurduc, D. Scutaru, J. Therm. Anal. Calorim. 83 (2006) 335.
[15] D. Apreutesei, G. Lisa, Natalia Hurduc, D. Scutaru, Scientific Study Res. VI (2005) 165.
[16] I. Carlescu, G. Lisa, D. Scutaru, J. Therm. Anal. Calorim. 91 (2008) 535.
[17] V.T. Yılmaz, A. Karada, H. Içbudak, Thermochim. Acta 261 (1) (1995) 107.
[18] X.-T. Li, J.-H. Li, G.-E. Zhang, G.-X. Xi, X.-D. Lou, Thermochim. Acta 262 (15) (1995) 165.
[19] A.C. de Souza, A.T.N. Pires, V. Soldi, J. Therm. Anal. Calorim. 70 (2002) 405.
[20] P. Budrugeac, Thermochim. Acta, in press.
[21] P.E. Sanchez-Jimenez, L.A. Perez-Maqueda, A. Perejon, J.M. Criado, Polym. Degrad. Stabil. 94 (2009) 2079.
[22] S. Vyazovkin, I. Dranca, X. Fan, R. Advincula, Macromol. Rapid Commun. 25 (2004) 498.
[23] D. Apreutesei, G. Lisa, H. Akutsu, N. Hurduc, S. Nakatsuji, D. Scutaru, Appl. Organomet. Chem. 19 (2005) 1022.
[24] D. Apreutesei, G. Mehl, D. Scutaru, Liq. Cryst. 34 (2007) 1.
[25] R. Deschenaux, J.W. Goodby, in: A. Togni, T. Hayashi (Eds.), Ferrocenes: Homogeneous Catalysis, Organic Synthesis Materials Science, VCH Weinheim, Germany, 1995 (Chapter 9).
[26] M. Moriyama, S. Song, N. Tamaoki, J. Mater. Chem. 11 (2001) 1003.
[27] D. Apreutesei, G. Lisa, D. Scutaru, N. Hurduc, J. Optoelectron. Adv. Mater. 8 (2006) 737.
[28] J. Pitkänen, J. Huttunen, H. Haltutunen, R. Vesterinen, J. Therm. Anal. Calorim. 56 (1999) 253.
[29] V.A. Korolev, O.M. Nefedov, Russ. Chem. Bull. 42 (1993) 1436.